

The Relationship of Surface Roughness and Work Function of Pure Silver by Numerical Modeling

Ye Wan^{1,2*}, Yanbo Li¹, Qing Wang¹, Ke Zhang³, Yuhou Wu³

¹ School of Materials Science and Engineering, Shenyang Jianzhu University, Shenyang 110168, China

² Department of Materials Science and Engineering, University of Virginia, Charlottesville, VA 22904, USA

³ School of Traffic and Mechanical Engineering, Shenyang Jianzhu University, Shenyang 110168, China

*E-mail: ywan@sjzu.edu.cn

Received: 28 March 2012 / Accepted: 6 May 2012 / Published: 1 June 2012

Surface of silver has important effects on its performance in natural environments. Surface roughness and work function of the silver samples were measured using confocal laser scanning microscopy and scanning Kelvin probe respectively. A model concerning the relationship of the surface roughness and work function was proposed. The objective is to provide a foundation for the effective use of numerical model about the relationship of the surface roughness and work function. The result showed work function decreased with surface roughness. Comparison between the experiments and the model about roughness and work function showed the model was in agreement with the experiments. The theoretical results of numerical model were obtained by computational approaches and based on Maple[®] codes.

Keywords: Silver; Work function; Surface roughness; Modeling study

1. INTRODUCTION

Work function (or surface potential for nonmetal) is one of the important properties of solid surfaces. Valence electrons are confined to the surface of metals by a surface potential barrier. Work function (WF), denoted by ϕ , is the difference of the rise in mean electrostatic potential across the metal surface and the bulk chemical potential of the electrons relative to the mean electrostatic potential in the metal interior. In other words, work function is equal to the minimum work that must be done to remove an electron from the surface of metal at 0 K [1], so it is a main factor decisive to the corrosion properties of materials. Lower WF can improve electron activities and raise corrosion rate, while higher WF corresponds to higher resistance to corrosion. WF can be easily measured by Kelvin

probe technique, which is a noncontact, nondestructive vibrating capacitor technique used to measure the work function difference ($\Delta\phi$) between a conducting tip and a conducting sample [2].

Surface roughness (SR), one basic parameter of surface condition, influences significantly the measured chemical, physical, dielectric, and mechanical properties of "real" materials [3-6]. Work function, a fundamental electronic property of a metallic surface, is extremely sensitive to surface conditions [7]. However, the study of the effect of SR on work function is rather rare. Some existing results showed [6, 8-10] that the larger SR is, the smaller WF is. In generally, this phenomenon was explained by SR effect on the dipole barrier [11]. At the same time, the effect of SR is often accompanied with other factors, such as oxidation and surface treatment. After the surface was treated, the effect of SR of the materials on their work function even showed opposite phenomena [12].

Silver is a very important metal because it has the highest electrical, the highest thermal conductivity and the highest reflectance in the visible and infrared spectral regions of all the metals [13]. WF of silver surface and its corrosion possibility are very important to its later usage in the atmospheres. WF of silver surfaces and the surface potential have been reported by the photoelectric methods [7, 14-16]. However, none of these WF investigations was an independent research made of SR because the scientists couldn't resolve the technical problems at that time. Although there were many phenomena showed there was some dependence of WF on silver surface, there were few quantitative data available for SR of silver.

So far, the detailed relationship of SR and WF of silver is not clear, and a comprehensive understanding of WF on silver is still not sufficient. In the present study, the silver surfaces with different SR were prepared. The relationship of SR and WF of silver were investigated with a numerical model as well. Moreover, a numerical model on the relationship between SR and WF of silver surface was deduced on the basis of a theoretical simulation.

2. EXPERIMENTAL

2.1 Confocal laser scanning microscopy measure

Confocal laser scanning microscopy (CLSM) was provided by Carl Zeiss Inc. (Thornwood, New York, USA) is a contact-free method [17-18] and can provide 3-D images and surface roughness. CLSM measurement was performed at the wavelength of 543 nm. The scan area, there was 512 points collected per line, of the instrument was set to $100\ \mu\text{m} \times 100\ \mu\text{m}$. SR can be characterized approximately by a mean height of irregularities about an average plane, and a correlation lengthening between irregularities [19]. The calculating method of SR for CLSM is the mean height of all surface height values and can be given basing on the Eq. (1) [20], which is a collection of statistical and mathematical methods that are useful to model and analyze SR.

$$S_a = \frac{1}{N_x \cdot N_y} \cdot \sum_{i=1}^{N_x} \cdot \sum_{j=1}^{N_y} \cdot z(x_i, y_j) \quad (1)$$

where N_x and N_y are the numbers of pixels in x -direction and y -direction, and $z(x_i, y_j)$ is the elevation for a given point.

2.2 Scanning Kelvin probe measure

WFs of silver samples with different surface roughness were carried out using a scanning Kelvin probe (SKP) system provided by KP Technology Ltd. (Caithness, UK). The samples were mounted in the SKP apparatus and allowed to equilibrate for a period of half an hour with an atmosphere at ca. 60% relative humidity (RH). A gold plated tip with a diameter of 2 mm was used and scanned a projected area uniformly. The tip moved 0.635 μm per step. The measurements (on different samples) were performed with the same gradient and with the sample space within 1 micron. The scanning area, covering 10 point \times 10 point in the experiment, was 6.35 mm \times 6.35 mm.

2.3 Materials

Fine silver samples of 75mm \times 15mm \times 0.25mm and 99.95% purity were obtained from Lucas-Milhaupt. Inc. (Cudahy, WI, USA). Some surfaces of silver samples were wet abraded with 120, 180, 240, 400, 600, 800 and 1200 grit grinding paper respectively. The others were prepared using 1200 grit grinding paper before they were polished with aqueous grinding paste solutions of 1 μm or 0.05 μm alumina respectively. All the silver samples with various surface roughnesses were followed by degreased with Alconox detergent and cleaned in deionized water, and dried in air for further measurement of SR and WF. There were some grooves along the polishing directions (Fig. 2).

3. MODELING

Simulations were run with the Maple[®] software, which solved problems with integral equations and plotting. WFs were measured with SKP, which principle [21] was to consider the electronic energy diagram for the surfaces of two dissimilar metals, which were separated by a distance d (shown in Fig.1). Before electrical contact was made, such as SW was open, the highest energy electrons in each metal occupied states at their respective Fermi level ϵ_{tip} and ϵ_s . φ_{tip} and φ_s were the WFs of the tip and the silver sample respectively, just as seen in Fig.1(a). If an external electrical contact was made between the tip and the silver sample, seen in Fig.1(b), electrons would flow from the metal with a lower WF to that with a higher WF until ϵ_{tip} equalized ϵ_s . Then Fermi levels of the two surfaces became equal and the two surfaces were oppositely charged. The corresponding flows of electrons produced a potential gradient (termed contact potential V_C).

Given,

$$V_C = (\varphi_{\text{tip}} - \varphi_s) / e, \quad (2)$$

where e was the electronic charge. Then,

$$\varphi_s = \varphi_{tip} - eV_c \tag{3}$$

And Q , the surface charge, was expressed as:

$$Q = V_c \cdot C_k = \frac{C_k}{e} (\varphi_{tip} - \varphi_s), \tag{4}$$

The tip vibrated periodically in the space, and its vibrating function could be expressed as $d_t = d_0' \cdot \cos\omega t$. Where ω and d_0' were the frequency and the amplitude of oscillation of the tip respectively. t was oscillation time. In generally, oscillation frequency of the tip of SKP was between 10 KHz - 20 KHz, which was much bigger than the moving velocity of the tip along x -direction and y -direction.

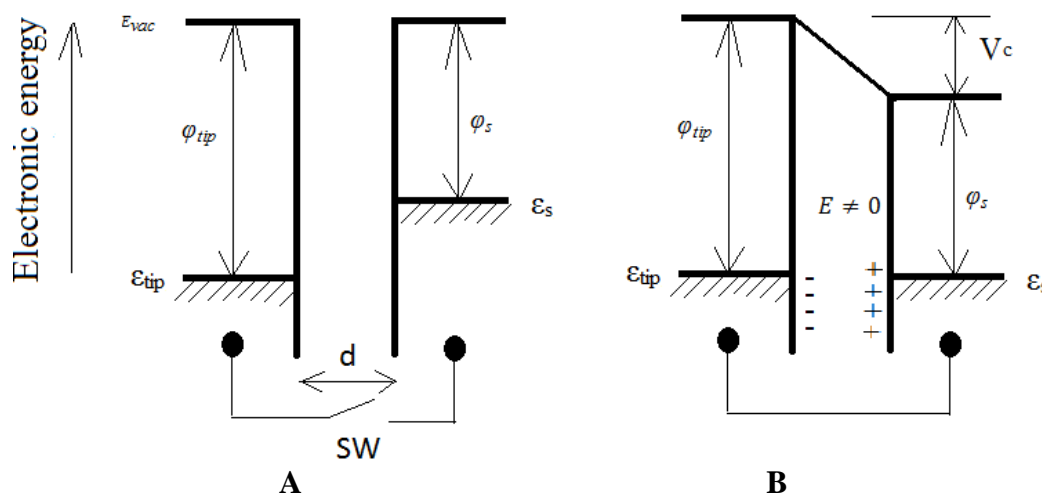


Figure 1. Electronic energy level diagrams for the tip and the sample separated by a distance d (a) before electrical contact (SW open), and (b) after contact. ϵ_{tip} , ϵ_s , and φ_{tip} , φ_s refer to the respective Fermi levels and work function for the tip and the silver sample.

In order to make the model simple, assuming:

(a) The tip moves at a stable flat plate. That means the amplitude and the vibrating frequency of the tip were constant. The micro capacitor formed between the length of the tip and the corresponding area on the surface of the sample is a flat parallel-plate capacitor. It gives:

$$C_k = \frac{\epsilon_0 \cdot \epsilon_r \cdot A}{d} = \frac{\epsilon_0 \cdot A}{d}, \tag{5}$$

where C_k is the capacitance of the capacitor. ϵ_0 is the vacuum permittivity in free space ($\epsilon_0 = 8.85 \times 10^{-12} \text{m}^{-3} \cdot \text{kg}^{-1} \cdot \text{s}^4 \cdot \text{A}^2$). ϵ_r is the relative permittivity in air ($\epsilon_r = 1$). A and d is the area and the distance between the tip and a given surface of the silver sample respectively (shown in Fig.2).

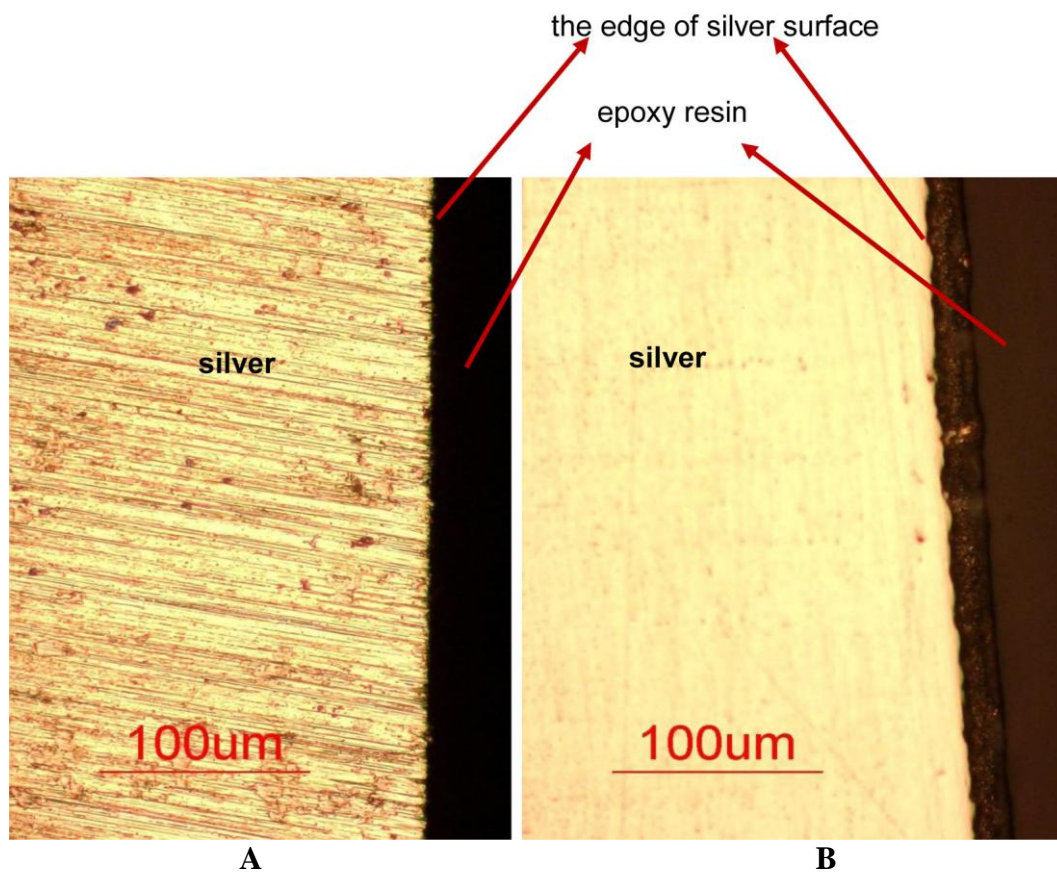


Figure 2. (a) microscope of the silver surface abraded with 600 grit paper, and (b) cross-section microscope of the silver surface abraded with 600 grit paper. The cross section was abraded with successively abrasive paper before the sample was polished with 0.05 μm alumina paste.

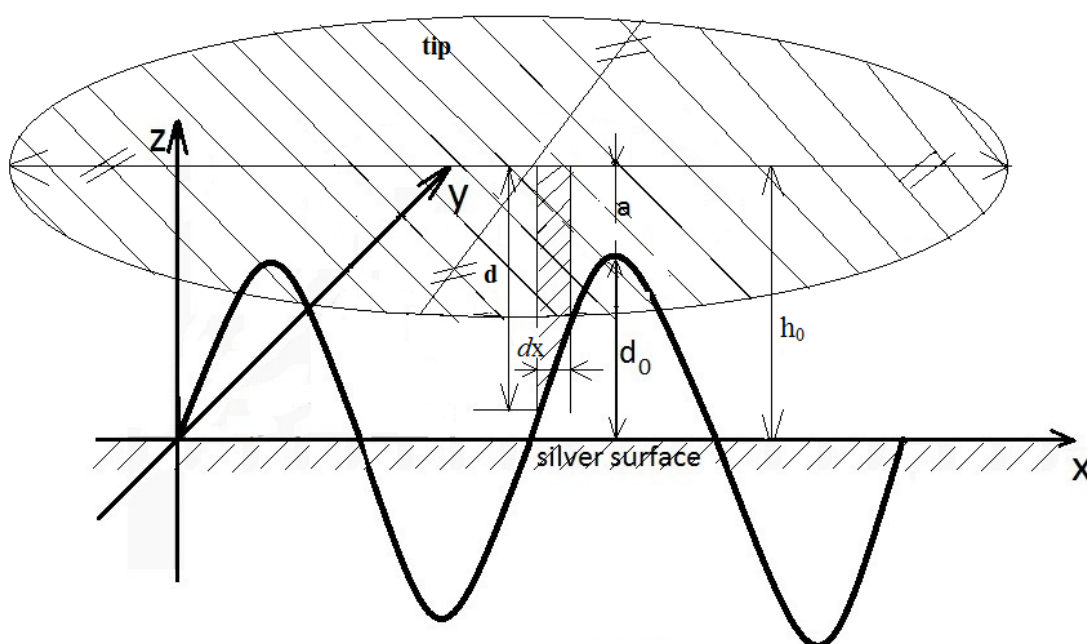
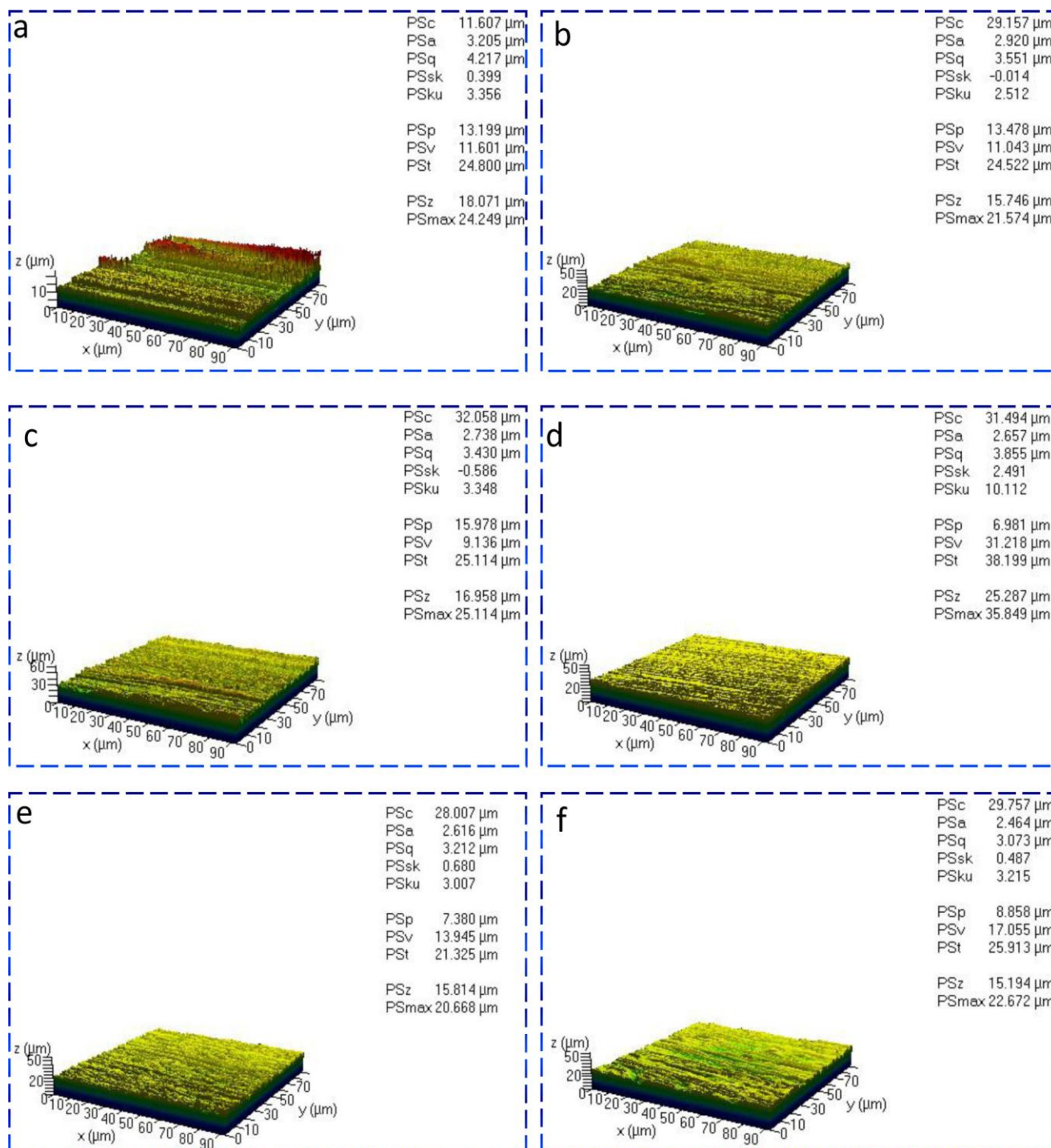


Figure 3. Schematic view of a parallel plate capacitor between the tip and the surface of the silver sample. Assuming the surface of silver is a periodical wave function along x-direction.

(b) $z(x, y)$, the elevation of a given point in the surface of the silver samples, shows a periodic fluctuation of the x -direction distance microscopically and y -direction is parallel to the groove direction. $z(x, y)$ can be expressed as $z(x, y) = d_0 \cdot \cos x$. d_0 is the periodic peak amplitude of the grooves created by polishing, on the silver surface (shown in Fig. 3).

It was reasonable that z was dependent of y because the abrading grooves on the surface were parallel to each other along the abrading direction of the sample (shown in Fig. 3 and Fig. 4).



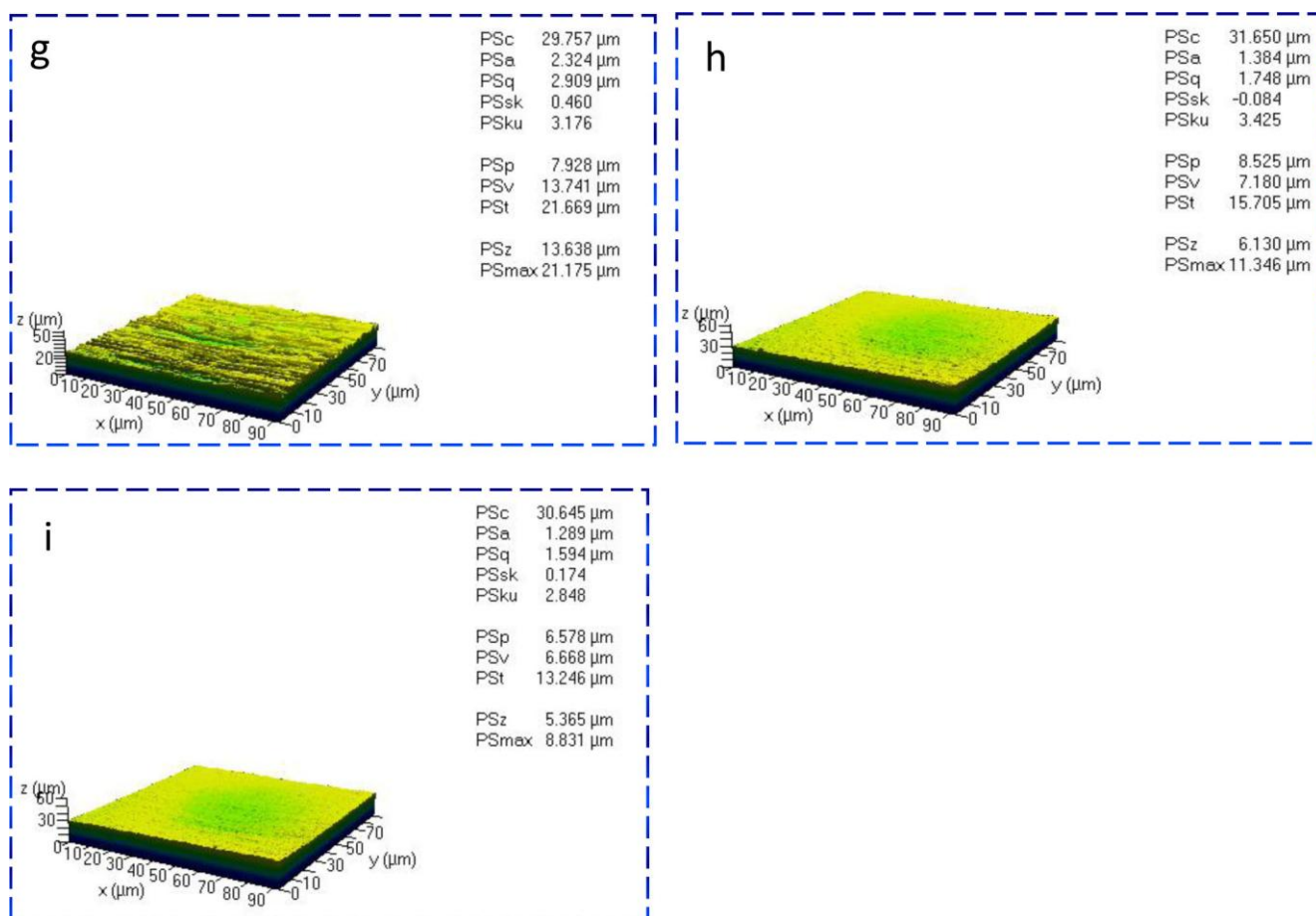


Figure. 4 The surface images and the measured surface roughness of the samples by the CLSM instrument. (a), (b), (c), (d), (e), (f) and (g) were those abraded with 120, 180, 240, 400, 600, 800, 1200 grit grinding paper respectively. While (h) and (i) were polished with 1μm and 0.05μm alumina grinding paste respectively.

As the area was continuous, the Eq. (1) could be expressed as the following integral function when the laser of the CLSM instrument scanned along *x*- and *y*- directions:

$$\begin{aligned}
 S_a &= \frac{1}{S_0} \iint |Z(x,y)| \cdot dx \cdot dy = \frac{1}{S_0} \iint d_0 \cdot |\sin x| \cdot dx \cdot dy = \frac{d_0}{S_0} \int_0^x |\sin x| \cdot dx \int_0^y dy \\
 &= \frac{d_0}{x \cdot y} \int_0^x |\sin x| \cdot dx \cdot \int_0^y dy = \frac{d_0}{x} \int_0^x |\sin x| \cdot dx
 \end{aligned}
 \tag{6}$$

S_0 was the projected area on the surface of the sample. SR can be calculated from a given scanning area of CLSM. *x* and *y* were the scanning distances of the laser in the CLSM instrument along *x*-direction and *y*-direction respectively. The unit of R_a was determined by the CLSM instrument and it was micron in the experiment.

Introduction of assumption (a) and (b) gave the expression (5) for a flat parallel-plate capacitor between a small area dS_0 and the opposite surface area on the tip:

$$dC_x = \frac{\epsilon_0 \cdot dS_0}{d} = \frac{\epsilon_0 \cdot dx \cdot dy}{h_0 - d_0 \cdot \sin x}
 \tag{7}$$

Basing on the assumption (b),

$$dC_k = \frac{\epsilon_0 \cdot dx \cdot dy}{h_0 - d_0 \cdot \sin x} = \frac{\epsilon_0 \cdot y_0 \cdot dx}{h_0 - d_0 \cdot \sin x} \tag{8}$$

$$C_k = \int dC_k = \int_{n_0 \cdot x_0}^{(n_0+1) \cdot x_0} \frac{\epsilon_0 \cdot y_0 \cdot dx}{h_0 - d_0 \cdot \sin x} = \epsilon_0 \cdot y_0 \cdot \int_{n_0 \cdot x_0}^{(n_0+1) \cdot x_0} \frac{dx}{h_0 - d_0 \cdot \sin x} \tag{9}$$

Here, h_0 was the average distance of the flat parallel-plate capacitor between the surface of silver sample and the gold tip (Fig. 2). x_0 and y_0 were the distances of a step of the tip of SKP along x -direction and y -direction respectively. n_0 was the steps of the tip of SKP along x -direction.

In an ideal condition, the whole surface of silver sample toward the gold tip was flat, then $d_0=0$, and $h_0=a$. a was the distance of the tip to the peak of the surface of the silver samples in Fig. 3. There is an ideal flat parallel-plate capacitor between silver sample and gold tip. The charge of the whole surface of the tip, can be expressed as the following:

$$Q_0 = C_{k0} \cdot \frac{(\varphi_{tip}^0 - \varphi_s^0)}{\epsilon} = \frac{\epsilon_0 \cdot A_0}{\epsilon \cdot a} \cdot (\varphi_{tip}^0 - \varphi_s^0) \tag{10}$$

where C_{k0} and A_0 are the capacitance and the surface area of the ideal flat parallel-plate capacitor between the surface of silver sample and the gold tip respectively. A_0 equals the surface area of the gold tip. φ_{tip}^0 and φ_s^0 are the WFs of the tip and the silver sample below the vacuum level. Q , the charge of the given area (S_0 , the area that the tip scans one step along x -direction and y -direction) on the surface of the silver sample, is proportional to the given area:

$$Q = \frac{\epsilon_0 \cdot A_0}{\epsilon \cdot a} (\varphi_{tip}^0 - \varphi_s^0) \cdot \frac{S_0}{A_0} = \frac{\epsilon_0 \cdot S_0}{\epsilon \cdot a} (\varphi_{tip}^0 - \varphi_s^0) = \frac{\epsilon_0 \cdot x_0 \cdot y_0}{\epsilon \cdot a} (\varphi_{tip}^0 - \varphi_s^0) \tag{11}$$

In order to get WFs in the given area of the silver sample, we inserted Eqs. (4), (9) and (11) into Eq.(3), giving:

$$\begin{aligned} \varphi_s &= \varphi_{tip} - eV_c = \varphi_{tip} - e \cdot \frac{Q}{C_k} = \varphi_{tip} - e \cdot \frac{\epsilon_0 \cdot x_0 \cdot y_0}{\epsilon \cdot a} \cdot (\varphi_{tip}^0 - \varphi_s^0) \cdot \frac{1}{\epsilon_0 \cdot y_0 \cdot \int_{n_0 \cdot x_0}^{(n_0+1) \cdot x_0} \frac{dx}{h_0 - d_0 \cdot \sin x}} \\ &= \varphi_{tip} - \frac{x_0}{a} \cdot (\varphi_{tip}^0 - \varphi_s^0) \cdot \frac{1}{\int_{n_0 \cdot x_0}^{(n_0+1) \cdot x_0} \frac{dx}{h_0 - d_0 \cdot \sin x}} \end{aligned} \tag{12}$$

(c) Because gold is a noble metal and $\epsilon_0 = \epsilon$, then,

$$\varphi_{tip}^0 = \varphi_{tip}$$

and

$$\varphi_s = \varphi_{tip} - \frac{x_0}{a} \cdot (\varphi_{tip}^0 - \varphi_s^0) \cdot \frac{1}{\int_{n_0 \cdot x_0}^{(n_0+1) \cdot x_0} \frac{dx}{h_0 - d_0 \cdot \sin x}} \tag{13}$$

φ_{tip}^0 and φ_s^0 are common for the materials of tip and samples. After x_0 is set, the expression of φ_s and S_a will be determined.

4. RESULTS AND DISCUSSION

4.1 Surface micromorphology

After prepared with different methods, the surfaces of the silver samples showed distinct patterns. The surface of the silver sample abraded with finer particle size of abrasive materials was much more burnishing than those with coarser abrasive materials. Fig.4 depicted the micro morphology of the silver samples abraded with different particle sizes of abrasive paper or paste. It showed that the surface of the silver sample abraded with finer particle size of grinding materials was much smoother. There were a lot of parallel grooves along the abrading direction in the micro-morphology, which verified the validation of the assumption (b) in section 3 as well. Surface roughness (PS_a in Fig. 4) was calculated by CLSM software after the CLSM system measured the micromorphology. The different grit abrasive papers or pastes were key factors influencing the surface condition of the samples. For example, S_a of the surface of the samples prepared with 120 grit grinding paper was 3.205 μm and it was 1.289 μm for the sample with 0.05 μm grinding paste. The particle sizes of the grinding papers and pastes were in the order: 120 grit > 180 grit > 240 grit > 400 grit > 600 grit > 800 grit > 1200 grit > 1 μm > 0.05 μm . The values of S_R were in the same order as the particle sizes of the grinding papers and pastes. The bigger was the particle size of the grinding paper or paste, the bigger was the values of S_a . S_a was the biggest for the surface of the samples abraded with 120 grit paper.

4.2 Work function of the silver samples

Table 1. The SRs and the mean WFs of silver abraded by different abrading materials

Abraded condition	experimental SR, μm	WF from the models, mV	experimental mean WF, mV
120 grit paper	3.205	2135.2	2514
180 grit paper	2.920	2310.1	2603
240 grit paper	2.738	2422.3	2721
400 grit paper	2.657	2472.4	2825
600 grit paper	2.616	2497.8	2875
800 grit paper	2.464	2592.1	2960
1200 grit paper	2.324	2679.3	3014
1 μm Al ₂ O ₃ paste	1.384	3276.5	3163
0.05 μm Al ₂ O ₃ paste	1.289	3338.4	3176

Table 1 showed the SRs and the WFs of the surface of the silver samples abraded with different particle sizes of grinding paper or paste by the SKP system. It could be seen from Table 1 that the SRs increased and the WFs decreased with the particle sizes of the abrasive materials. The values of WF demonstrated that WF was dependent on the surface roughness of silver samples. That was because a rougher surface had lower constraint for electrons to escape from peaks, resulting in lower WF and consequently higher corrosion rates [22]. The results on the corrosion rate of different WF and different surface roughness will be shown in a later research paper.

4.3 Model validation

Recall that the SR model and the calculated S_a in Eq. (6), it could be seen that there were two main factors affecting the value of S_a . One was d_0 , which depended on the abrasive paper. It could be seen from Eq. (6) that the bigger was d_0 , the bigger was S_a . Therefore, the bigger was the particle size of the abrasive paper or paste, the bigger was the values of S_a , which was in agreement with the experimental results in Fig.3 from CLSM. The other main factor affecting S_a was the scanning distance (x) of the laser in the image instrument. The absolute value of $\sin(x)$ in Eq. (6) depended on the value of x . SR is a relative quantity and depends on the ratio of length scale of the irregularities to the wavelength of the laser [23], which relies on the accuracy of the instrument. Since x was set to 100 μm in the experiment,

$$S_a = \frac{63 \cdot d_0 + d_0 \cdot \cos 100}{100} = 0.6283 \cdot d_0. \tag{14}$$

However, if x is set to 635 μm ,

$$S_a = \frac{405 \cdot d_0 - d_0 \cdot \cos 635}{635} = 0.6364 \cdot d_0. \tag{15}$$

Eq. (9) showed the relationship of the scanning step of SKP tip and capacitance. x_0 , the distance of a step of the SKP tip, was set to 0.635 μm in the CLSM instrument. Assume $n_0=1$, then Eq. (9) can be described as the following:

$$C_k = - \frac{2 \cdot \varepsilon \cdot y_0 \cdot \left[\arctan\left(\frac{0.829 \cdot h_0 - d_0}{\sqrt{h_0^2 - d_0^2}}\right) - \arctan\left(\frac{0.787 \cdot h_0 - d_0}{\sqrt{h_0^2 - d_0^2}}\right) \right]}{\sqrt{h_0^2 - d_0^2}} \tag{16}$$

Because the tracking system of SKP could hold automatically the distance to be 0.3175 μm between the tip and the sample, and the diameter of the tip (2mm) was much bigger than the scanning distance of the CLSM, a was 0.3175 μm and h_0 was $(0.3175 + d_0)$. From Eq. (14), $d_0 = \frac{S_a}{0.6283}$. Note that the average surface potentials of silver and gold below the vacuum level were $\varphi_s^0 = 4260 \text{ meV}$ and $\varphi_{tip}^0 = 5100 \text{ meV}$ respectively [24], the model concerning the relationship between φ_s and S_a was as the following:

$$\varphi_s = 5100 + \frac{840 \cdot (0.1 + 1.024 S_a)^{\frac{1}{2}}}{\arctan \left[\frac{-0.104 + 1.088 S_a}{(0.1 + 1.024 S_a)^{\frac{1}{2}}} \right] - \arctan \left[\frac{-0.284 + 0.424 S_a}{(0.1 + 1.024 S_a)^{\frac{1}{2}}} \right]} \quad (17)$$

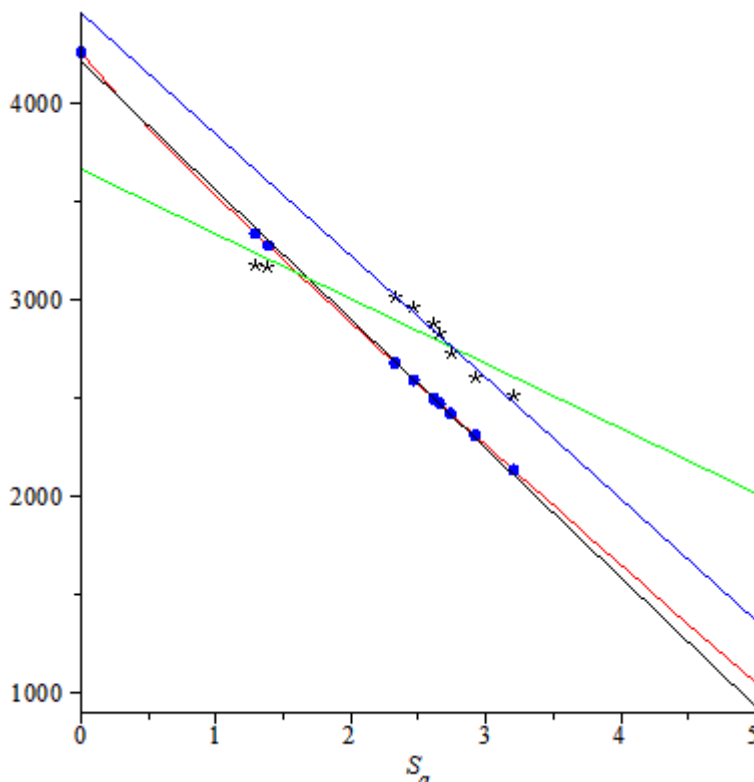


Figure 5. Comparison of the experimental WF profiles obtained by SKP (black stars) with the simulated WFs (blue plots, the black line is leastsquares linear fitting by those blue plots) and the simulated curve (red line) profiles obtained by simulating numerical model at different SRs. The green line was leastsquares linear fitting of the experimental WF of the samples abrading from 120 grit abrading paper to 0.05µm polishing paste, while the blue line was that from 120 grit to 1200 grit abrading paper.

Fig.5 showed the simulated relationship of WF and SR of the silver surfaces abraded with different grit papers. The simulation was run with the Maple[®] software. The experimental WFs were also plotted in Fig.5. The red line was the curve drawn according to Eq. (17). The black line was the leastsquares linear fitting curve of the blue plots calculated by Eq. (17) when SRs were from 1.289 µm to 3.205µm. The black stars were the experimental WFs of the surfaces with different SRs and shown in Fig.5. The green line was leastsquares linear fitting curve basing on the experimental WFs of the surfaces with different SRs. The blue line was leastsquares linear fitting curve basing on the experimental WFs of the surfaces with SRs from 3.205 µm to 1.289 µm.

The equation for the leastsquares linear fitting was:

$$\varphi_s = m - n \cdot S_a. \quad (18)$$

m was the extreme value of WF of silver at different environment. n stood for the speed of the changes of WFs of the silver surfaces at different surface roughness. The values of m , n and R were listed in Table 2. R was the correlation coefficient of the leastsquares linear fitting curves. The values of R showed that WF decreased linearly with S_a in the experiments. It could be seen from Table 2 that the changing trend of WF in Eq. (17) was very familiar with that of the experimental WF of silver surfaces when SRs were from 3.205 μm to 2.324 μm .

Table 2. Parameters of m , n and R of linear fitting formula $\varphi_s = m - n \cdot S_a$

	m	n	R
Eq (17)	4219.4	657.9	0.9999
Experimental WFs for the SRs from 2.324 to 3.205	4460.4	618.8	0.9806
Experimental WFs for all the SRs	3664.2	330	0.9302

The standard deviation (SD) of n from Eq. (17) to the experimental WFs (when SRs were from 2.324 μm to 3.205 μm) was 6.3% and the model was valid at the condition. One of the reasons why there was a deviation might be because there was periodic fluctuation of the surfaces being simulated the charge in the capacitor. However, n from Eq. (17) deviated far away from the experimental WFs of silver surfaces with all of the SRs. The error of n was $\frac{657.948 - 329.965}{329.965} \times 100\% = 99.4\%$. When SR was too big, d_0 was too big to make a parallel plates, and the plates couldn't be considered as a parallel-plate capacitor any more. It could be seen from the values of m , there were also some effects of the boundary condition on WF of silver. The value of m in Eq. (18) was closer to WFs of the surfaces when SRs were from 1.289 μm to 3.205 μm than that with SRs from 2.324 μm to 3.205 μm . The smoother was the surface and the smaller was the difference of m between the model and the experimental values. If the grinding paper were too coarse or too fine, there were the boundary conditions to calculate WF in the model.

WF could be interpreted easily from surface roughness of silver. If the surface of silver was rough, the electrons on the surface of the silver samples were easy to depart from the peaks of the grooves. That is, it kept a lower WF. Since the grooves were parallel to the grinding direction (shown in Fig. 2 and Fig. 4) of the samples, a uniform distribution of WF along the grinding direction was expected. WFs measured in SKP system also verified the results and the validation of the assumption (b) in the section 3. It was noted that the simulated values were lower than the experimental ones. The difference between simulated values and experimental values might be attributed to the surrounding environments. The WFs from Eq. (16) were based on the average surface potentials of silver and gold below the vacuum level. However, the experimental WFs were in the 60% RH atmosphere. These should be another reason there were some difference between WF from the model and the experiments.

5. CONCLUSIONS

Based on the theories of flat parallel-plate capacitor and the surface roughness, a numerical model of the relationship of WF and SR was deduced. The numerical model revealed that WFs of the surfaces of the silver samples decreased linearly with S_a . The experimental results demonstrated that WF decreased linearly with SR of silver surface. The numerical model deduced from the software might be used to detect the value of SR or WF after one of them was decided, and could be used to calculate the depth of the groove on the polished surface of the silver samples as well.

ACKNOWLEDGMENTS

This work was supported by grants from D. Dunmire, Director of Corrosion Policy and Oversight, Office of the Secretary of Defense, NSFC Projects 51101106 and 51131007. The discussions with Prof. Kelly are gratefully acknowledged. Special thanks go to Dr. George W.G. Booth about WF, Wasiu Adedeji about the discussion of surface roughness and Lok-kun Tsui for the usage of Maple software and the debugging of the model.

References

1. N. D. Lang and W. Kohn, *Phys. Rev. B*, 3 (1971) 1215-1223
2. I. D. Baikie, and P.J.S. Smith, *Rev. Sci. Instrum*, 69 (1998) 3902-3907
3. D.E. Aspnes, J.B. Theeten, and F. Hottier, *Phys. Rev. B*, 20(1979)3292-3302
4. R.S. Sirohi, *Opt. Commun*, 1 (1970) 304-306
5. E.C. Chan and J.P. Marton, *J. Appl. Phys*, 45 (1974) 5004-5007
6. W. Li and D.Y. Li, *J. Chem. Phys*, 122 (2005) 064708
7. M. Chelvayohan and C.H.B. Mee, *J. Phys. C: Solid State Phys*, 15 (1982) 2305-2312
8. R. Ozawa, K. Kaykham, A. Hiraishi, Y. Suzuki, N. Mori, T. Yaguchi, J. Itoh and S. Yamamoto, *Appl. Surf. Sci*, 146 (1999) 162-168
9. J. S. Kim, F. Cacialli and M. Granstrom, *Synthetic. Met*, 101 (1999) 111-112
10. T.A. Beierlein, W. Brutting, H. Riel, E.K. Haskal and W. Rieβ, *Synthetic. Met*, 111-112 (2000) 295-297
11. S. Saito, K. Takeda, T. Soumura, T. Tani and T. Maeda, *Phys. Status Solidi A*, 142 (1994) K29-K32
12. Y. B. Zhao and R. Gomer, *Surf. Sci*, 250 (1991) 81-89
13. H.E. Bennett, R.L. Peck, D.K. Burge and J.M. Bennett, *J. Appl. Phys*, 40 (1969) 3351-3360
14. M. Uda, A. Nakamura, T. Yamamoto and Y. Fujimoto, *J. Electron Spectrosc*, 88-91 (1998) 643-648
15. P.A. Anderson, *Phys. Rev*, 59 (1941) 1034-1041
16. H.E. Farnsworth and R.P. Winch, *Phys. Rev*, 58 (1940) 812-819
17. M.A. Alodan and W.H. Smyrl, *J. Electrochem. Soc*, 144 (1997) L282- L284
18. J.B. Pawley, *Handbook of Biological Confocal Microscopy*, 2nd ed., Plenum Press, New York (1995)
19. P. Beckmann, *The depolarization of Electromagnetic Waves*, Golem Press, Boulder (1968)
20. Carl Zeiss Inc, *LSM 510 Laser Scanning Microscopy Operating Manual*, Carl Zeiss Inc.: USA, 2000
21. I. D. Baikie, P.J.S. Smith, D.M. Porterfield and P.J. Estrup, *Rev. Sci. Instrum*, 70 (1999) 1842-1850
22. X.Y. Wang and D.Y. Li, *Electrochim. Acta*, 47 (2002) 3939-3947
23. D.E. Aspnes, J.B. Theeten and F. Hottier, *Phys. Rev. B*, 20 (1979) 3292-3302
24. R.C. Weast, *CRC Handbook of Chemistry and Physics*, 69th ed., CRC (Chemical Rubber Corp.) Press, Florida (1988)